LIMNOLOGY and OCEANOGRAPHY

ASLO

Limnol. Oceanogr. 9999, 2020, 1–18
© 2020 The Authors. *Limnology and Oceanography* published by Wiley Periodicals LLC on behalf of Association for the Sciences of Limnology and Oceanography.
doi: 10.1002/lno.11620

Water temperature control on CO_2 flux and evaporation over a subtropical seagrass meadow revealed by atmospheric eddy covariance

Bryce R. Van Dam,[1,2*] **Christian C. Lopes**,[2] **Pierre Polsenaere**,[3] **René M. Price**,[4] **Anna Rutgersson**,[5] **James W. Fourqurean**[2]

[1]Institute of Coastal Research, Helmholtz-Zentrum Geesthacht (HZG), Geesthacht, Germany
[2]Department of Biological Sciences and Center for Coastal Oceans Research, Florida International University, Miami, Florida
[3]IFREMER, Laboratoire Environnement Ressources des Pertuis Charentais (LER-PC), La Tremblade, France
[4]Department of Earth and Environment and Southeast Environmental Research Center, Florida International University, Miami, Florida
[5]Department of Earth Sciences, Uppsala University, Uppsala, Sweden

Abstract

Subtropical seagrass meadows play a major role in the coastal carbon cycle, but the nature of air–water CO_2 exchanges over these ecosystems is still poorly understood. The complex physical forcing of air–water exchange in coastal waters challenges our ability to quantify bulk exchanges of CO_2 and water (evaporation), emphasizing the need for direct measurements. We describe the first direct measurements of evaporation and CO_2 flux over a calcifying seagrass meadow near Bob Allen Keys, Florida. Over the 78-d study, CO_2 emissions were 36% greater during the day than at night, and the site was a net CO_2 source to the atmosphere of 0.27 ± 0.17 μmol m^{-2} s^{-1} ($x\bar{c} \pm$ standard deviation). A quarter (23%) of the diurnal variability in CO_2 flux was caused by the effect of changing water temperature on gas solubility. Furthermore, evaporation rates were $\sim$ 10 times greater than precipitation, causing a 14% increase in salinity, a potential precursor of seagrass die-offs. Evaporation rates were not correlated with solar radiation, but instead with air–water temperature gradient and wind shear. We also confirm the role of convective forcing on night-time enhancement and day-time suppression of gas transfer. At this site, temperature trends are regulated by solar heating, combined with shallow water depth and relatively consistent air temperature. Our findings indicate that evaporation and air–water CO_2 exchange over shallow, tropical, and subtropical seagrass ecosystems may be fundamentally different than in submerged vegetated environments elsewhere, in part due to the complex physical forcing of coastal air–sea gas transfer.

Shallow seagrasses of the tropics and subtropics are highly productive ecosystems, supporting economically and ecologically important food webs in surrounding regions. Seagrass meadows also cover and protect belowground organic carbon stocks which are significant to the global carbon cycle (Duarte et al. 2005; Fourqurean et al. 2012*a*; Fourqurean et al. 2012*b*). While these "blue carbon" reservoirs contain significant amounts of seagrass-derived carbon, nonseagrass autochthonous and autochthonous material often composes around 50% of this blue carbon stock (Kennedy et al. 2010; Röhr et al. 2018). During periods of high seagrass primary production and CO_2 consumption, the water column partial pressure of CO_2 (pCO_2) may fall below that of the atmosphere, causing a net transfer of atmospheric CO_2 into the water (Perez et al. 2018). Given the relative ease with which dissolved oxygen (DO) can be measured, ecosystem metabolic rates are often assessed with DO, which is converting into units of carbon assuming a specific O_2: CO_2 ratio (Duarte et al. 2010). Recent underwater O_2 eddy covariance studies have yielded well-resolved measurements of seagrass production (Long et al. 2015), showing that some seagrass systems are near metabolic balance (Attard et al. 2019) or can shift between autotrophy and heterotrophy (Berg et al. 2019). Benthic chamber-based DO studies have also shown net heterotrophy at some sites (Asmala et al. 2019). This use of DO as a proxy for CO_2 may be appropriate in siliciclastic and noncalcifying systems (Attard et al. 2019), where the ratio of

*Correspondence: vandam.bryce@gmail.com

This is an open access article under the terms of the Creative Commons Attribution-NonCommercial License, which permits use, distribution and reproduction in any medium, provided the original work is properly cited and is not used for commercial purposes.

Author Contribution Statement: J.W.F., C.C.L., and B.R.V.D. conceived of the study, B.R.V.D. designed the research methodology and formal analysis for this study, while field and lab work were carried out by B.R.V.D. and C.C.L. The original draft of this manuscript was prepared by B.R.V.D., while further review and editing was conducted by C.C.L., P.P., A.R., R.M.P., and J.W.F.

O_2: CO_2 consumption may be near 1: 1. However, in carbonate-dominated systems, changes in total alkalinity due to $CaCO_3$ formation and dissolution along with anaerobic alkalinity inputs will cause pCO_2 changes independent of O_2. In net calcifying systems (common among tropical and subtropical seagrass), metabolic rates estimated using DO may be biased toward autotrophy, to an extent that is proportional to the ratio of net ecosystem production to calcification (Van Dam et al. 2019*a*). Likewise, DO-based methods may underestimate metabolism when carbonate minerals are being dissolved. Consequently, there is a clear need for direct measurements of air–water CO_2 exchanges in tropical and subtropical seagrasses. Such measurements, in conjunction with rigorous ecosystem metabolism studies, may begin to help resolving the question of whether these important ecosystems are sources or sinks of carbon to the atmosphere.

The subject of air–water CO_2 exchange over seagrasses has received much attention in recent years, owing in large part to the emerging interest in coastal vegetated habitats as carbon sinks (the concept of "blue carbon"; Nellemann et al. 2009), and the growing recognition of calcification as a potential confounding factor (Howard et al. 2018). Understanding air–water CO_2 exchange above seagrass meadows is key to their importance in global carbon budgets, yet few studies have measured CO_2 fluxes over seagrasses, and nearly all have taken place in temperate, tidally influenced systems (Polsenaere et al. 2012; Tokoro et al. 2014). The only prior measurements of CO_2 flux in Florida Bay (with floating domes) found clear regions of CO_2 emission and uptake throughout the bay (DuFore 2011), but lacked assessment of diel variability, thus presenting an incomplete picture of CO_2 exchanges and ecosystem metabolism. Because of the difficulty in directly measuring CO_2 flux, it is often estimated by combining measured pCO_2 with an empirical parameterization attempting to capture the physical forcing of turbulence at the air–water interface. However, the factors governing air–water gas exchange in these shallow, wind-exposed, and often fetch-limited systems are poorly understood and likely site-specific.

While wind is clearly an important driver of gas transfer in coastal waters (Upstill-Goddard 2006), especially when water is relatively deep (Ho et al. 2018*a*), other factors like bottom-driven turbulence (Tokoro et al. 2007; Ho et al. 2016, 2018*b*), convective forcing (Rutgersson et al. 2011; Czikowsky et al. 2018; Van Dam et al. 2019*b*), biological surfactants (McKenna and McGillis 2004; Ribas-Ribas et al. 2018), and wave slope (Wanninkhof et al. 2009) may cause variations in gas transfer irrespective of wind.

Underpinning this diverse forcing of gas transfer is the physical structure of the air–water interface, which is bounded on both sides by diffusive sublayers in the air and water. The exchange of gas across this boundary is rate-limited by diffusion through each of these sublayers, although for gasses of relatively low solubility (e.g., CO_2, CH_4), the resistance is largely on the water side. While the size of the water-side diffusive sublayer is typically considered most sensitive to wind-driven mixing, other factors like convection and bottom-generated turbulence can be key when conditions are calm (Upstill-Goddard 2006; Wanninkhof et al. 2009). As a result, well-established wind- and current-based gas transfer parameterizations developed for the open ocean (Jiang et al. 2008; Wanninkhof 2014) and coastal waters (Ho et al. 2016) may not apply in seagrass meadows, where thermal forcing, surfactants, and other factors can affect variations in gas transfer independent of wind speed. This uncertain physical forcing of gas transfer has challenged prior efforts to constrain CO_2 fluxes over tropical and subtropical seagrasses, which make up the largest fraction of seagrass area globally (Green and Short 2003). Therefore, direct measurements of CO_2 flux in these "blue carbon" systems are highly desirable (Macreadie et al. 2019), especially when combined with a rigorous assessment of gas transfer.

In addition to investigating seagrass ecosystem productivity and carbon storage, air–water turbulent fluxes are also relevant to other factors affecting seagrass ecosystem health. For example, seagrasses in shallow and tropical waters are sensitive to extreme temperatures, with die-offs typically occurring during warm late summer months (Zieman et al. 1989; Robblee et al. 1991; Koch et al. 2007). The causes of these die-offs are varied and complex, but are made worse during conditions of high water temperature and hyper-salinity, which reduce O_2 solubility and allow H_2S gas to accumulate to toxic levels (Borum et al. 2005). Therefore, a better understanding of the factors affecting salinity and temperature over seagrass meadows is relevant to the prospect of future seagrass die-offs. In areas with little freshwater inputs through surface or groundwater channels, like Florida Bay, seasonal and event-scale variations in salinity are driven by the relative rates of evaporation and precipitation (Nuttle et al. 2000; Swart and Price 2002; Lee et al. 2006), and by water mass advection, when salinity is spatially variable. Direct measurements of evaporation are not yet available for Florida Bay, and model estimates show methodological uncertainty (Lee et al. 2006; Price et al. 2007).

In this study, we used atmospheric Eddy Covariance to make the first direct measurements of CO_2 and H_2O (evaporation) exchanges in Florida Bay, a well-studied seagrass-dominated system. Our objective was to identify the dominant physical and biogeochemical processes governing turbulent fluxes over shallow submerged seagrasses. We describe a set of unique drivers that causes air–water CO_2 exchange in this system to differ from results in seagrass meadows elsewhere. Evaporation rates (latent heat fluxes) are also assessed and placed into the context of past and potential future seagrass die-offs. We also use heat transfer as a proxy for the gas transfer velocity, enabling the first preliminary assessment of the potential physical drivers of gas exchange in shallow subtropical seagrasses. Collectively, our findings support the role of temperature as a critical driver of air–water CO_2 and

latent heat exchange. These findings improve our understanding of air–sea CO_2 and H_2O exchange in seagrasses, clarifying the role of tropical and subtropical seagrass ecosystems in broader regional and global carbon and water cycles.

Methods

Site description

Florida Bay is a large and shallow embayment stretching between the Florida Keys and the coastal Everglades. Fine carbonate mud throughout the bay is colonized by mixed seagrasses (mostly *Thalassia testudinum*, also *Halodule wrighti*, and *Syringodium filiforme*) and calcareous green macroalgae (Zieman et al. 1989). Primary producers are heavily phosphorus-limited to the northeast, but P delivered by tidal exchange with the Gulf of Mexico supports greater primary production in western Florida Bay (Fourqurean et al. 1992; Armitage and Fourqurean 2016) This study took place near the center of this P-limited productivity gradient (Fig. 1), near Bob Allen keys (5.027 N 80.681 W). Here, a shallow basin of 1–2 m depth is surrounded by mud banks which significantly restrict tidal exchange (Wang et al. 1994). Tidal amplitudes (~ 0.05 m) and water currents (< 2 cm s^{-1}) are very low, and are driven by winds rather than lunar tides (Holmquist et al. 1989; Long et al. 2015).Water residence times in this region of Florida Bay are 6–12 months (Lee et al. 2006). Rates of net ecosystem metabolism (Long et al. 2015) and belowground organic carbon stocks are moderate for the Bay (Fourqurean et al. 2012*b*), despite phosphorus-limited seagrass primary production (Armitage and Fourqurean 2016). Underwater O_2-based eddy covariance measurements made in 2012 (Long et al. 2015) showed that the gross primary productivity of the benthic community at Bob Allen Keys (151 ± 23 mmol O_2 m^{-2} d^{-1}) was intermediate of sites to the east (Duck [68 ± 6 mmol O_2 m^{-2} d^{-1}]) and west (Rabbit Key Basin [190 ± 27 mmol O_2 m^{-2} d^{-1}]).

Eddy covariance and biometeorological measurements

Our eddy covariance system (Li-Cor, U.S.A.) was installed on an existing permanent data collection structure operated by the Everglades National Park at Bob Allen keys (water quality station BOBF1). This eddy covariance system consists of a rapidly responding (10 Hz) closed-path infrared gas analyzer (Li-7200RS), a sonic anemometer (Gill Windmaster Pro), and bio-meteorological sensors for net solar radiation (Kipp & Zonen NR Lite2), photosynthetically active radiation (PAR; Li-190R Quantum Sensor), and precipitation. Wind speed was corrected to a height of 10 m (U_{10}) assuming neutral

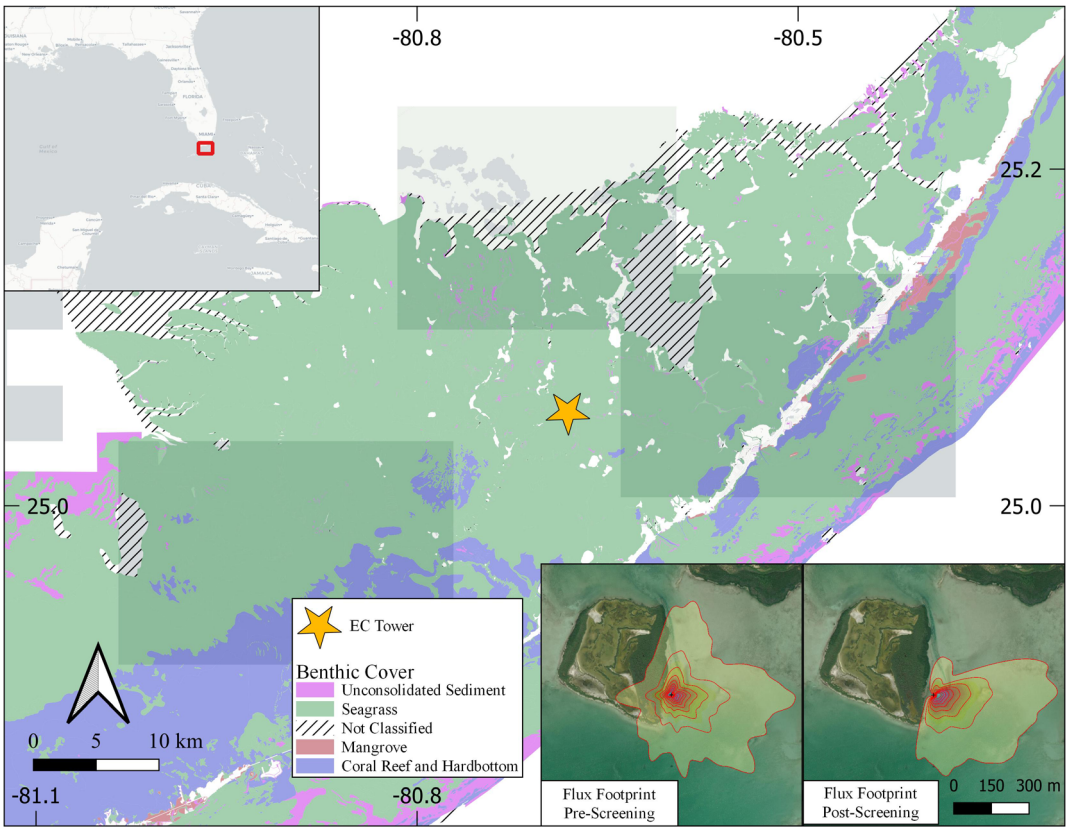

Fig. 1. Site map and eddy covariance footprint analysis (FFPonline tool; Kljun et al. 2015), showing the impact of data screening steps ("Data post-processing and screening" section) on the spatial representativeness of eddy covariance flux data. Red lines represent contours of flux contribution in increments of 10%. Benthic coverage data acquired from Florida Fish and Wildlife Conservation Commission, unified reef map.

conditions (Large and Pond 1981). Additional parameters such as water depth, temperature, and salinity were measured hourly by the Everglades National Park staff at the same location. Hourly average water temperature and salinity records were linearly interpolated to 30 min to match the measurement frequency of the other results. Eddy covariance instrumentation was operational from 22 March 2019 until 07 June 2019, for a total of 78 d. Air–water fluxes of CO_2, latent heat, and sensible heat were determined from high-frequency (10 Hz) measurements of CO_2, H_2O and temperature, and were calculated at 30-min intervals using an automated routine in EddyPro (Li-Cor). Equations used for calculating latent heat, sensible heat, and CO_2 fluxes are described in Foken et al. (2012). Positive latent and sensible heat fluxes represent heat loss from the water. In order to more comprehensively assess the energy balance, we also estimated the water-column heat storage (J; W m^{-2}) for each 30 min interval as:

$$J = (\rho \times C_{p^o} \times \Delta T / \Delta t \times h) \quad (1)$$

where ρ is the average water density for that time period (kg m^{-3}), C_{p^o} is the specific heat of water (J kg^{-1} K^{-1}), $\Delta T/\Delta t$ is the average rate of water temperature change (K s^{-1}), and h is the water depth (m). While this approach necessarily ignores the heat flux into sediments and any lateral advection, information is lacking to estimate these fluxes. In order to assess the role of water-side convective forcing on CO_2 and latent heat fluxes, we calculated buoyancy flux (B) according to Czikowsky et al. (2018). First, the effective heat flux (Q_{eff}) was calculated as the downwelling net solar radiation (R_n) minus the latent (LE) and sensible (H) heat fluxes.

$$Q_{eff} = R_n - H - \mathrm{LE} \quad (2)$$

The buoyancy flux (B; m^2 s^{-3}) was calculated as in Podgrajsek et al. (2015):

$$B = g\alpha Q_{eff} / \rho C_{pw} \quad (3)$$

where g (m s^{-2}) is the gravitational acceleration, α (unitless) is the thermal expansion coefficient, and C_{pw} (J kg^{-1} K^{-1}) is the specific heat of water. When calculated in this manner, positive buoyancy fluxes indicate a loss of density from the water, which thereby becomes more buoyant. The result of this is greater stratification and an increasing stability of the sea surface microlayer, which can hamper rates of gas transfer. On the other hand, when buoyancy flux is negative, there is a gain in density at the water surface, enhancing convective overturn, and thereby gas transfer. We then converted all negative values of buoyancy flux (equation not valid for buoyancy fluxes > 0) into a water-side convective velocity scale (w_{*w}, m s^{-1}) according to the equation (Jeffery et al. 2007; Van Dam et al. 2019*b*):

$$w_{*w} = \sqrt[3]{-Bh} \quad (4)$$

Data postprocessing and screening

Postprocessing of high-frequency data in EddyPro involves a variety of steps including tilt correction, time-lag compensation, Webb-Pearman-Leuning corrections (Webb et al. 1980), as well as high/low pass filtering. In addition to these steps, the 30-min data were further screened by a variety of criteria intended to ensure that final data were representative of the appropriate flux footprint (i.e., the calculated footprint given wind speed and direction only contained the intended focus area, the submerged seagrass ecosystems), and to exclude times when conditions were nonstationary (i.e., statistics of flow are consistent through time), or when the IRGA optics appeared dirty. These conditions, the problem each criterion seeks to remedy, and the quantity of data lost to each criterium are shown in Table 1. The quality control procedure implemented by EddyPro (Mauder and Foken 2006) has become an internationally standard approach to postprocessing of eddy covariance data (see FLUXNET and AmeriFlux), and we have adopted the same approach here.

Table 1. Criteria used to screen eddy covariance data, including brief justification and fraction of measurements that did not meet each step (*see* "Eddy covariance and biometeorological measurements" section for a description of screening variables).

Criteria	Threshold for data rejection	Reason for rejection	Percent of 30-min data failing this criteria
Wind direction	$\theta > 200$	Footprint mismatch	22%
EddyPro QC code	QC code > 0	Calculated fluxes failed standard postprocessing (Mauder and Foken 2006)	33%
ΔSignal Strength	ΔSIGNAL Strength > 1.7	Suspect dirty IRGA optics	7%
$\lvert CO_2 \text{ flux}\rvert$	$\lvert CO_2 \text{ flux}\rvert > 3$ μmol m^{-2} s^{-1}	Anomalous CO_2 flux	7%
z/L	$z/L < -0.55$	Excessive instability	4%
u_*	$u_* < 0.1$	Insufficient turbulence	11%
CO_2/H_2O variance	>0.3 ppm	Poor precision from Li-7200RS	14%
Total			43%

The QC code generated by EddyPro ranges from 0 (no suspected issues) to 2 (flux results highly suspect), and we took the conservative approach of only using flux results when the QC code was flagged as "0." This screening procedure was the most common cause of data loss, accounting for 33% of rejected flux data. Data failing the EddyPro QC threshold also often failed other criteria, which collectively accounted for the removal of 43% of records.

It was also important to screen data when atmospheric conditions were excessively unstable. Lower atmospheric stability can be assessed quantitatively through Monin-Obukhov similarity theory, where the length scale L (m) is the height above the sea surface at which shear and buoyant forcing are equally important. When L is less than the measurement height (z), the turbulent processes measured there are influenced by buoyant, rather than shear forcing. Therefore, we can use the ratio of z/L as an indicator of the relative importance of shear and buoyant forcing (Smedman et al. 2007). When z/L is greater than 0, the boundary layer is stable, and vertical transfer is driven by wind-shear. Negative values indicate convective, unstable conditions. Hence, we screened data that fell below a z/L threshold of −0.55 (Czikowsky et al. 2018), as described in Table 1. The intent of this step was to remove time periods when turbulent exchanges were influenced by regions outside of the intended flux footprint, due to excessive convective forcing and minimal wind shear. Such conditions accounted for the rejection of 4% of records, were evenly distributed between day and night, and occurred exclusively when wind was below 5 m s^{-1}. Last, the size of the eddy covariance flux footprint increases with z/L, such that the footprint may become problematically large (extending outside of the intended focus area) when z/L exceeds 0.15 (Mørk et al. 2014). Maximum z/L during the study period was 0.146, suggesting that such nonstationary and footprint mismatch issues were unlikely. The cumulative effect of all of our data screening procedures can be seen graphically in Fig. 1, where the eddy covariance flux footprint initially intersected with the mangrove island to the west, before data screening. Following our screening procedure, the flux footprint was limited to the relatively homogeneous area just east (< 500 m) of the eddy covariance tower, with a benthic cover of patchy seagrass (*Thalassia testudinum* and *Halodule wrightii*) and calcareous green macroalgae in 1–2 m water (Fig. 1, inset).

Physical drivers of CO_2 and latent heat fluxes

Air–water gas exchange can be expressed using a "bulk transfer" relationship where F_{gas} is the gas flux across the sea surface (measured by eddy covariance in this study), ΔC is the concentration difference between the water and air, and k_w is the gas transfer velocity:

$$F_{gas} = k_w \times \Delta C \tag{5}$$

While a rigorous assessment of gas transfer requires waterside measurements of CO_2 concentration (not measured in this study), it may still be possible to estimate k_w and investigate its drivers using air–water exchange of heat as a proxy for gas transfer. Prior studies have found positive relationships between the rate of air–water heat transfer (k_g) and that of air–water gas transfer (k_w), although k_g often exceeds k_w (Zappa et al. 2003). Given this general relationship between k_g and k_w, our direct measurements of air–water heat exchange (sensible + latent) can be used to estimate k_w (Wanninkhof et al. 2009). As an extension of Eq. 5, heat transfer can be parameterized as:

$$F_{heat} = k_g \times \Delta T \tag{6}$$

where ΔT is the water–air temperature gradient and F_{heat} is the net heat flux (sensible + latent). Rearranging Eq. 6, we can calculate k_g as follows:

$$k_g = F_{heat}/\Delta T \tag{7}$$

We can then convert k_g into a gas transfer velocity (k_w) according to Schmidt (Sc) to Prandtl (Pr) scaling:

$$k_w = k_g \times {}^{Sc}\!/_{Pr}{}^{-0.5} \tag{8}$$

Values of k_w less than 0 cm h^{-1} were excluded from subsequent analyses due to heat fluxes being inconsistent with air–water temperature gradient. While gas transfer velocities above 50 cm h^{-1} have been observed under high wind speed and wave-breaking conditions in the open ocean (Smith et al. 2011) and during storms in Fjords (Mørk et al. 2016), such conditions did not occur in this study, causing us to exclude $k_w > 50$ cm h^{-1} as outliers (Jonsson et al. 2008).

In situ measurements

In addition to the micrometeorological measurements described previously, a variety of hydrographic and biogeochemical sensors were deployed at the eddy covariance tower over varying intervals. First, an upward-facing Acoustic Doppler Current Profiler (ADCP) was deployed at the base of the tower, but given the shallow water depth (< 2 m), all ADCP bins were combined into a water-column average speed and direction. Additionally, a Datasonde capable of measuring temperature and salinity (EXO2, Yellow Springs International, U.S.A.) was deployed at the tower over various intervals, covering a total of 129 h. A direct comparison of our temperature and salinity measurements with those from the Everglades National Park showed a linear relationship with a slope of 1.0 ± 0.3 and an r^2 of > 0.96, and as such, we used our measurements to gap-fill when Everglades National Park data were absent or faulty. Unless otherwise noted, all error values are reported as mean ± standard deviation (SD).

Results

Energy balance

Over the study period, this site was a net source of sensible and latent heat to the atmosphere, with an average sensible and latent heat fluxes of 15.1 ± 13.8 W m^{-2} ($x\bar{c}$ ± SD) and 100.5 ± 51.8 W m^{-2}, respectively (Fig. 2c). Latent and sensible heat fluxes were positive for 99.9% and 90% of measurements, respectively, and heat fluxes were dominated by latent heat flux, which was greater than the sensible flux 99% of the time. The Bowen ratio (sensible flux: latent flux) was therefore quite low, with an average of 0.15 ± 0.18 ($x\bar{c}$ ± SD), typical of shallow tropical waters (Polsenaere et al. 2013; Rey-sánchez et al. 2017). The energy budget exhibited very poor closure (slope < 0.2) under the simple assumption that net solar radiation is balanced only by the sum of sensible and latent heat fluxes (Fig. 2a). However, when the heat storage term (*J*) is included as an energy sink, the slope indicating energy closure is nearly 1: 1, indicating better energy balance closure (Fig. 2b). Water-column energy storage due to solar heating is therefore an important component of the energy budget, as clearly endorsed by the large diel signature in water temperature (Fig. 3b). The mean evaporation rate (3.6 ± 1.8 mm d^{-1}; $x\bar{c}$ ± SD) was an order of magnitude greater than precipitation (0.32 ± 4.4 mm d^{-1}; $x\bar{c}$ ± SD), in close agreement with prior estimates for the Florida Bay dry season (Price et al. 2007). Further evidence for net evaporation can be seen in the salinity and temperature record, which shows a clear trend of increasing water temperature, rising from 20.34°C to 33.56°C and salinity, which rose ~ 14% from 37.19 to 42.25 over the study period (Fig. 3).

Temporal trends in air–water CO_2/latent heat fluxes and associated parameters

A footprint analysis (Kljun et al. 2015) indicated that an area less than 100 m east of the eddy covariance tower provided the majority (83%) of CO_2 flux measurements (Figs. 1, 4a). While CO_2 flux was generally distributed evenly across wind directions, it was slightly greater in the window of 70–90°. In this narrow window, U_{10} was also slightly higher (Fig. 4b), offering a partial explanation for the increase in CO_2 flux. Nevertheless, the flux footprint for this data set was generally homogeneous and dominated by seagrass beds overlain by a ~ 1.5 m water depth (Fig. 1). Mean U_{10} was moderate, at 6.6 ± 1.8 m s^{-1} ($x\bar{c}$ ± SD), and the presence of the trade winds prevented any development of diel cycle in wind speed or direction. Maximum U_{10} during the study period was 13.6 m s^{-1}. Over the study period, the majority of 30-min records of *z/L* (1631 out of 2588, or 63%) were within the unstable but very close to neutral (UVCN) zone (Fig. 5). These conditions of moderate atmospheric stability have been

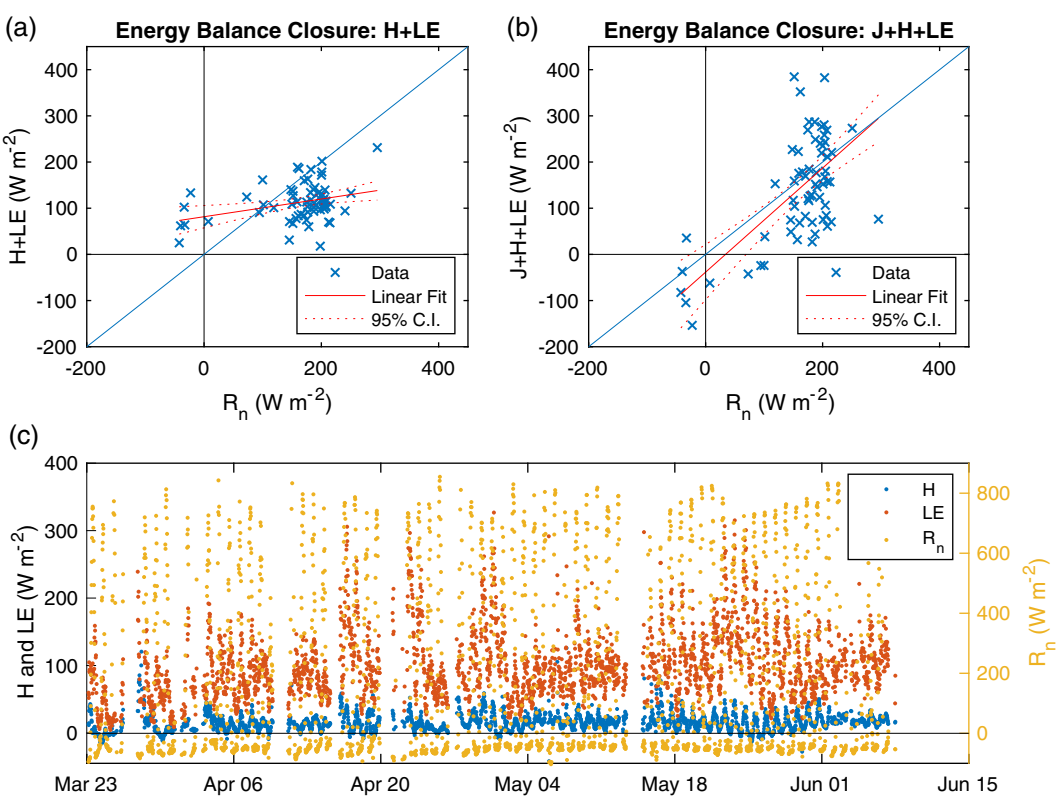

Fig. 2. Daily energy balance closure, where the water column heat storage term, *J*, is either excluded (**a**; $y = 0.19x + 81.6$; $R^2 = 0.11$) or included (**b**; $y = 1.1x - 38.4$; $R^2 = 0.41$). Time series plot of sensible (H) and latent (LE) heat fluxes, as well as net solar radiation (R_n) (**c**).

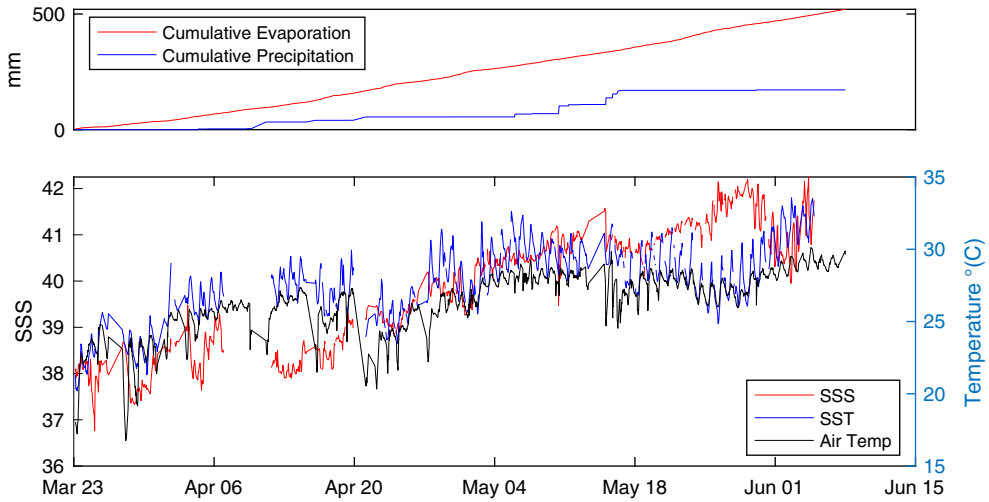

Fig. 3. (a) Time-series plot of cumulative evaporation and rainfall (mm), and **(b)** sea surface salinity (SSS), sea surface temperature (SST), and air temperature.

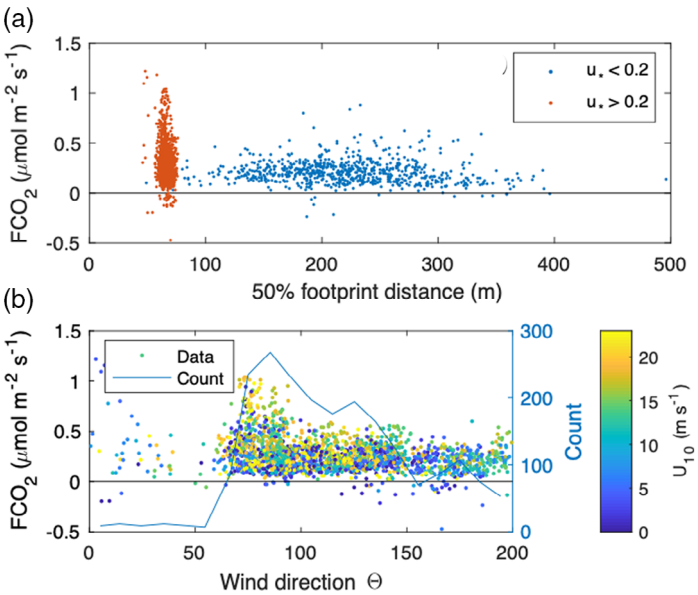

Fig. 4. Scatter plot of flux contribution distance and CO_2 flux (FCO_2), with points colored blue for $u_* < 0.2$, and orange for $u_* > 0.2$ (**a**). The difference between the patch at a footprint of ~ 75 m, and the footprint patch between 100 and 400 m is caused by the footprint calculation in EddyPro, which switches between two different algorithms at a u_* threshold of 0.2 m s^{-1}. FCO_2 as a function of wind direction, with points colored by U_{10} (**b**).

implicated in relative gas transfer enhancement (Smedman et al. 2007; Sahlée et al. 2008; Andersson et al. 2018), and we develop this concept in greater detail later in the "Discussion" section.

Water temperature was almost always greater than air temperature, and the average daily range in water temperature (2.8°C) was greater than the diel range in air temperature (2.0°C). As a result, the air–water temperature gradient ($\Delta T = T_{water} - T_{air}$) was almost always positive and increasing throughout the day, from a dawn minima to a dusk maxima, mirroring the trend in water temperature (Fig. 6d). The likely cause of this was the dominance of easterly "trade" winds. Air parcels reaching the site were therefore of a marine origin, with stable temperatures reflecting thermal equilibrium with ocean water, rather than a typical signature of daytime solar heating over land.

Over the study period, this site was a net source of CO_2 to the atmosphere, with an average CO_2 flux of 0.27 ± 0.17 μmol m^{-2} s^{-1} ($x\bar{c} \pm$ SD). Daytime CO_2 emissions (0.29 ± 0.17 μmol m^{-2} s^{-1}; $x\bar{c} \pm$ SD) was 17% greater than the nighttime CO_2 release (0.25 ± 0.17 μmol m^{-2} s^{-1}; $x\bar{c} \pm$ SD), and the only observed period of net CO_2 uptake occurred between 02 and 05 May, following a storm that generated high winds, relatively low water temperature, and no measurable rain. This period of CO_2 uptake was limited only to nighttime hours and was offset by CO_2 emissions during the day. A short period of CO_2 uptake was also observed during the nighttime hours of 24–25 March, when water temperature was near the minimum for the study period. While the study site was affected by many other storm events and generated at times significant rainfall rates and/or high wind speeds, they had no clear impact on trends in CO_2 flux.

Diel variability in both CO_2 and latent heat flux were large, typically around 0.15 μmol m^{-2} s^{-1} and > 100 W m^{-2}, respectively (Fig. 5). Hourly variations in CO_2 flux were also out of phase with PAR, which peaked around 12:00 h (Fig. 6b), compared with the CO_2 flux maxima near 15:00 h. Maximum CO_2 flux was typically just before sunset, while minimum CO_2 flux was often near sunrise. The large diel variability in ΔT coincided with a strong diel excursion in latent heat flux (Fig. 6b), such that peak latent heat flux (18:00 h) occurred at

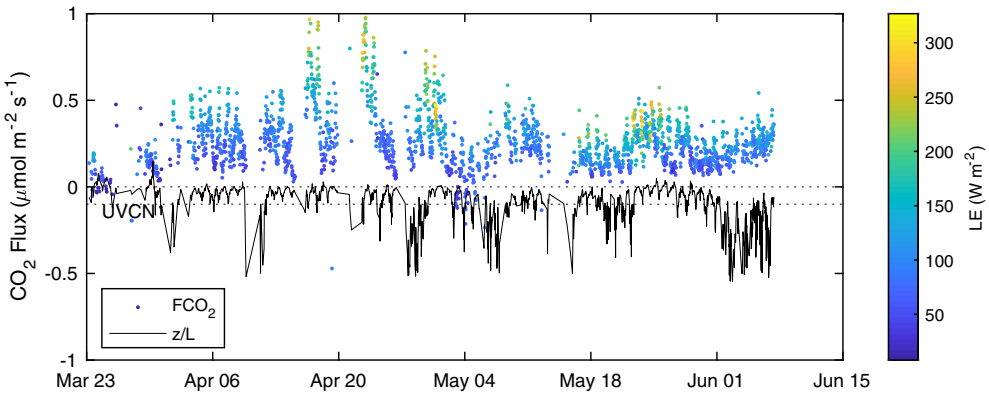

Fig. 5. Time-series plot of CO_2 flux (FCO_2) and z/L. FCO_2 values are colored by latent heat flux (LE), highlighting the positive correlation between these two fluxes. The UVCN zone ($-0.1 < z/L < 0$) is shown between the dotted horizontal lines.

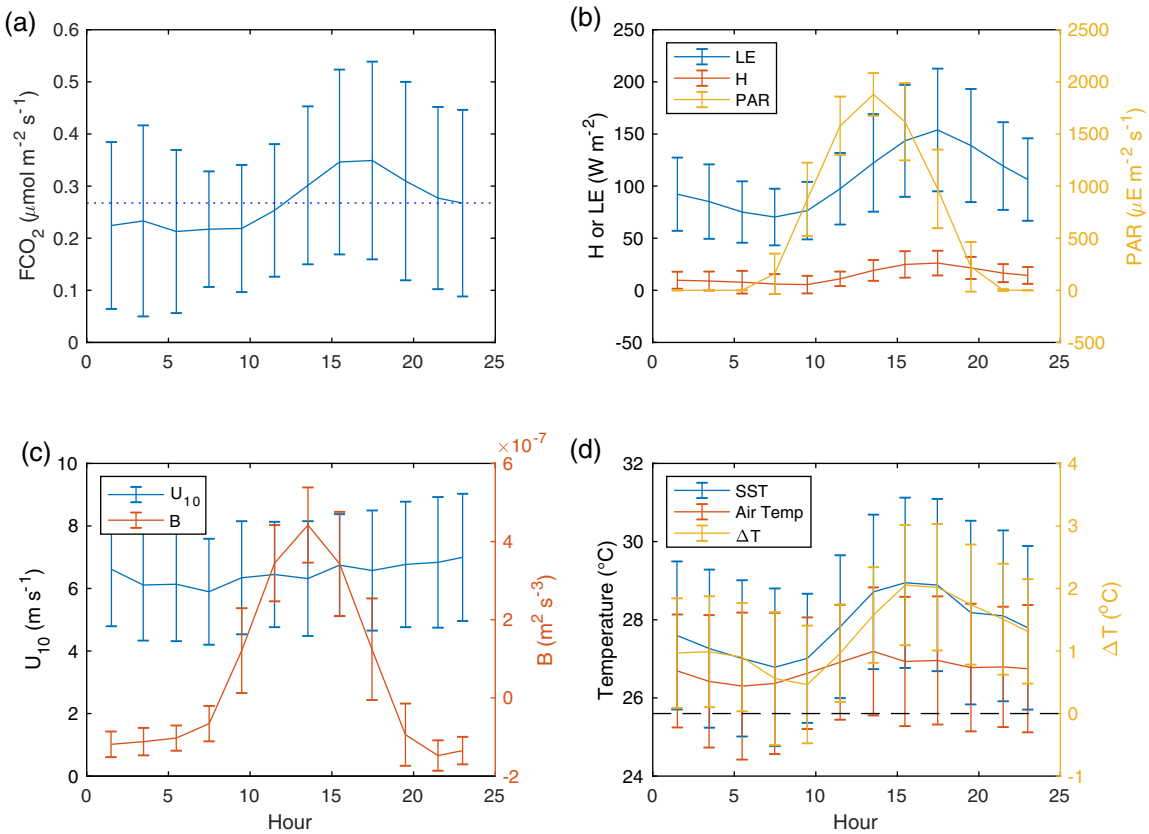

Fig. 6. Climatological hourly means for CO_2 flux (FCO_2) (**a**), energy balance terms sensible heat flux (H), latent heat flux (LE), and PAR (**b**), U_{10} and buoyancy flux (B) (**c**), and SST, air temperature, and ΔT ($T_{water} - T_{air}$) (**d**). Positive values of LE, H, and FCO_2 indicate release to the atmosphere. Error bars in this figure represent mean ± SD.

the same time as maximum water temperature, after PAR (and net solar radiation, not shown) has already peaked and begun to decrease. Buoyancy flux exhibited a diel trend similar to that in PAR and net solar radiation (not shown) with a maximum gain in buoyancy during the middle of the day, and buoyancy loss (convection) at night (Fig. 6c).

Correlations between measured fluxes and physical drivers

While prior studies have found net solar radiation to be a good predictor of evaporation in Florida Bay (Price et al. 2007) and in the large and shallow lake Taihu, China (Lee et al. 2014) and Lake Erie, U.S.A. (Shao et al. 2015), we found weak correlations between latent heat flux and net solar radiation

($R^2 < 0.1$; root mean squared error = 50.1). Instead, latent heat flux was best predicted by an exponential function of water-side convection (w_{*w}) explaining 33% of the variability in latent heat flux. Likewise, significant positive correlations were found between latent heat flux and vapor pressure deficit, ΔT (Liu et al. 2009), and U_{10}. The strength of the correlation between latent heat flux and w_{*w} may be inflated due to the fact that latent heat flux itself is included in the calculation of w_{*w}. The correlation between latent heat flux and air temperature was very poor ($R^2 = 0.01$), while that with water temperature was slightly better ($R^2 = 0.07$), further indicating that variations in ΔT were dominated by water temperature variations, rather than air temperature. The interactive effects of wind and temperature on latent heat fluxes can be clearly seen in Fig. 7c, where at a given wind speed, latent heat flux increases with increasing temperature.

It was necessary to present absolute values of CO_2 flux ($|CO_2$ flux$|$) in Fig. 7e–h because the occasional negative CO_2 flux measurements (CO_2 uptake) would have obscured the relationship between the various physical drivers and CO_2 flux. The strongest correlations for $|CO_2$ flux$|$ were with w_{*w} ($R^2 = 0.13$) and U_{10} ($R^2 = 0.10$), while less predictive power was provided by ΔT and vapor pressure deficit ($R^2 < 0.10$). A linear correlation between CO_2 and latent heat flux ($R^2 = 0.37$) was also evident, reinforcing the concept that latent heat and CO_2 fluxes shared common physical drivers. Last, ADCP water velocity was not correlated with fluxes of CO_2 or latent heat, indicating that bottom-driven turbulence is at most a secondary driver of turbulent fluxes ($p < 0.05$; $R^2 = 0.013$ for CO_2 flux and $R^2 < 0.01$ for latent heat flux). While there was a significant negative linear relationship between water depth and CO_2 flux (increasing CO_2 flux with decreasing water depth), this correlation was weak ($r^2 < 0.1$) perhaps due to the very narrow tidal range at this site. Together, these relationships suggest that wind-shear and convective forcing were the dominant drivers of turbulent fluxes, exceeding the impact of bottom-generated turbulence.

Variations in estimated gas transfer velocity (k_w)

In this study, we used heat transfer as a proxy for gas transfer to make the first estimates of k_w over a seagrass meadow. This k_w compares well with three commonly used gas transfer models: Wanninkhof 2014 (k_{W14}), Jiang et al. 2008 (k_{J08}), and Ho et al. 2016 (k_{Ho16}) when considered as an average over the study period (Fig. 8a), and also captures much of the same short-term variability (Fig. 8b). The inclusion of current speed and water depth into the model (only k_{Ho16}) also yielded gas transfer velocities similar to our calculated k_w, but only for the $\sim$ 2.5 d for which ADCP data were available (Fig. 8b). Together with the poor relationship between CO_2 flux and water velocity, this finding suggests that bottom-generated turbulence was not a significant driver of air–water gas exchange.

In fact, the average difference between our calculated k_w and the models: k_{W14}, k_{J08}, or k_{Ho16} was not significantly different from zero, at -0.78 ± 9.0 cm h^{-1} ($k_w - k_{W14}$; $\bar{x} \pm$ SD), 0.55 ± 8.5 cm h^{-1}($k_w - k_{J08}$), and -3.6 ± 9.3 cm h^{-1}($k_w - k_{Ho16}$).

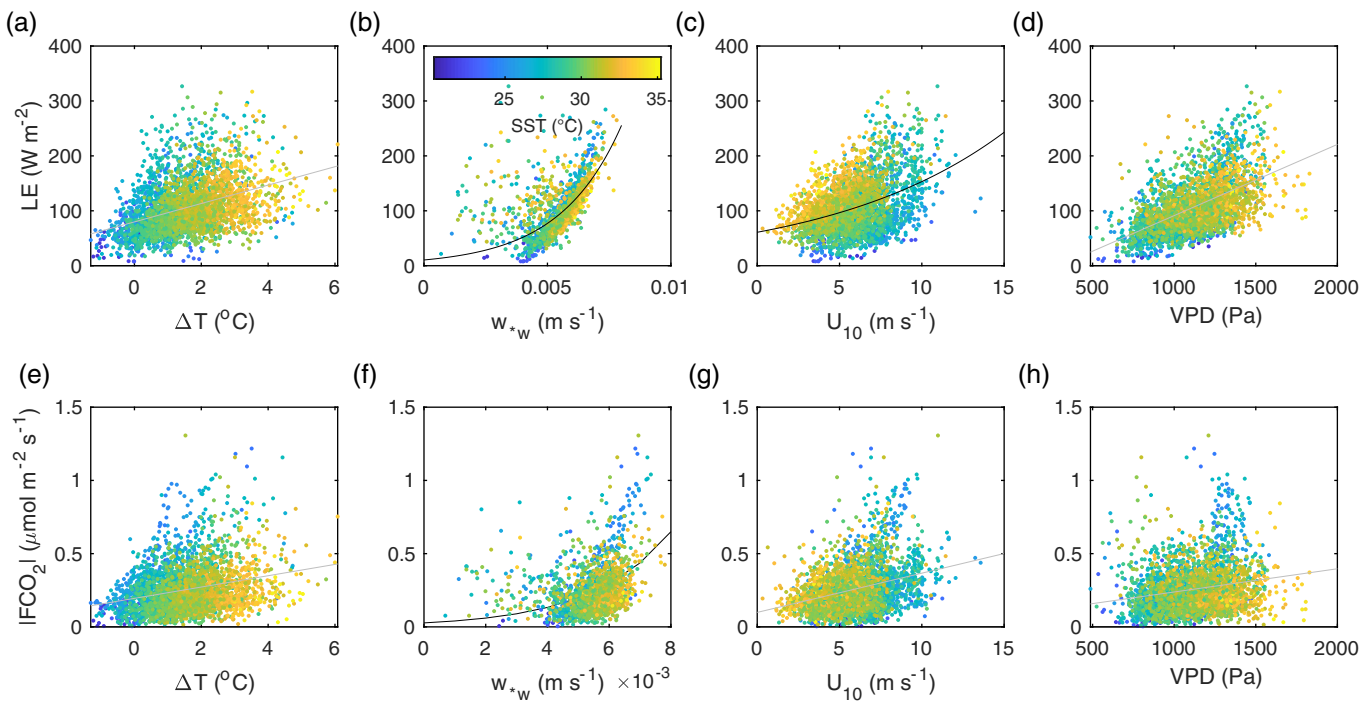

Fig. 7. Scatter plots showing potential drivers of latent heat flux (LE) (**a**–**d**) and absolute value CO_2 flux ($|FCO_2|$) (**e**–**h**), where the points are colored by SST. VPD, vapor pressure deficit.

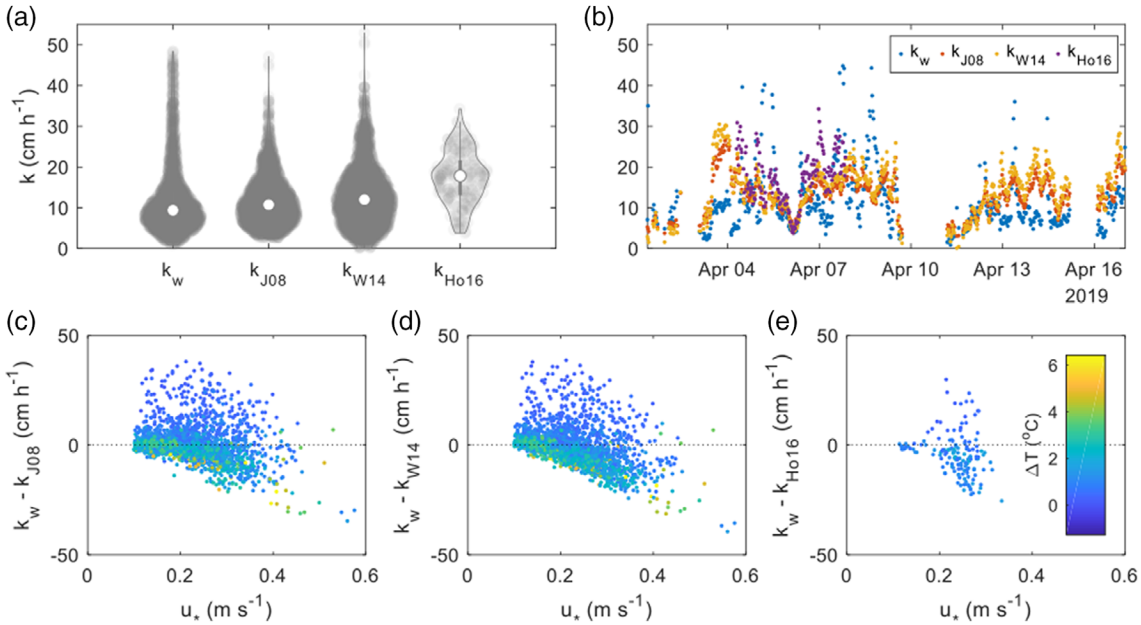

Fig. 8. Violin plot (**a**) of mean k_w (estimated from heat fluxes, at in situ Sc), compared with gas transfer models (k_{W14}, k_{J08}, k_{Ho16}), showing all records from the study period. ADCP current data were only available for a short period, explaining the small sample size for the Ho16 parameterization which considers water velocity. Selected time-series for 2 weeks in early April 2019 (**b**). Figures (**c**–**e**) show the difference between estimated and parameterized k_w as a function of the friction velocity (u_*), with points colored by ΔT.

Table 2. Best fit models (linear or exponential) for latent heat flux (LE) and absolute value CO_2 flux ($|FCO_2|$), for the set of drivers shown in Fig. 7. Vapor pressure deficit is abbreviated here as VPD. All equations presented have slopes significantly different from zero ($\alpha = 0.05$).

	LE		$\lvert CO_2$ flux$\rvert$	
	Model	R^2	Model	R^2
ΔT	$y = 16.75 \times \Delta T + 79.8$	0.15	$y = 0.039 \times \Delta T + 0.19$	0.07
w_{*w}	$y = 10.5\, e^{399 \times w_{*w}}$	0.33	$y = 0.027\, e^{397 \times w_{*w}}$	0.13
U_{10}	$y = 60.92\, e^{0.09 \times U_{10}}$	0.16	$y = 0.027 \times U_{10} + 0.099$	0.10
VPD	$y = 0.13 \times \text{VPD} - 38.3$	0.32	$y = 0.00016 \times \text{VPD} - 0.080$	0.04

This agreement between parameterized and calculated k_w further supported wind as a driver of gas transfer in shallow waters. However, it was also apparent that these parameterizations tended to over-predict k_w when wind-shear was high. This effect is evident in Fig. 7c,d, where the difference between calculated and modeled k ($k_w - k_{W14}$ and $k_w - k_{J08}$) becomes more negative with increasing u_*. This overprediction was greatest when ΔT exceeds 2–3°C, indicating that these common models of gas transfer may overpredict k_w, especially during the day as water heats relative to the air.

Discussion

Temperature-dependence of summer CO_2 flux in Florida Bay

We documented persistently high temperature differences between air and water (ΔT) throughout the study period. The likely cause of this was intense solar heating of shallow water, combined with easterly "trade winds" delivering maritime air masses of consistent temperature. Coinciding with this diel variability in ΔT, we also observed a large diel range in latent heat flux and CO_2 flux, which were both greatest in the late afternoon and at a minimum near sunrise (Fig. 6b). Not only were diel trends in CO_2 flux large, they were of opposite phase of what has been observed in other, noncarbonate, seagrass systems (Polsenaere et al. 2012; Tokoro et al. 2018). We also observe a significant positive correlation between CO_2 flux and ΔT (Fig. 7e), although the strength of this correlation was weak relative to U_{10} and w_{*w} (Table 2). The reason for this correlation between CO_2 flux and ΔT is unclear, but could be related to factors like the temperature-dependence of pCO_2 (Takahashi et al. 1993), or the temperature sensitivity of ecosystem respiration and calcification/dissolution. While robust

carbonate chemistry measurements are required to fully address this question, we can easily estimate a general thermal impact on pCO_2 variability. First, if we assume air–water CO_2 equilibrium, we can use the average atmospheric CO_2 concentration from this study (401.5 μatm) as an initial pCO_2 to which we can apply an isochemical temperature dependence of $\partial \ln(pCO_2)/\partial T = 0.0423°C^{-1}$ (Takahashi et al. 1993). This temperature sensitivity has an empirical relationship with salinity, ranging from 0.0332 at a salinity of 0–5 (Joesoef et al. 2015) to 0.0423 at a salinity of 36 (Takahashi et al. 1993). Combining this with the average daily range in water temperature over the study period (2.31°C), we can estimate a temperature-driven pCO_2 increase of 10.28% [$\exp(0.0423 \times (2.31\ ^\circ C)) = 1.1028$], or an increase of 41.3 μatm from the initial pCO_2 of 401.5 μatm. Using an average gas transfer velocity (k_w) from this study (11.7 cm h^{-1}, or 0.117 m h^{-1}) and CO_2 solubility (26.1 μmol m^{-3} μatm^{-1}), this pCO_2 increase should enhance CO_2 flux by $26.1 \times 41.3 \times 0.117 = 126.1$ μmol m^{-2} h^{-1}, or 0.035 μmol m^{-2} s^{-1}. This thermal effect can explain a similar magnitude decrease in CO_2 flux as water cools over the evening. The average diel range in CO_2 flux during the study was ~ 0.15 μmol m^{-2} s^{-1}, meaning that this thermal pCO_2 effect can explain 0.035/0.15, or $\sim$ 23% of the typical range in CO_2 flux over the study period.

While this thermal effect is clearly significant, a separate source of CO_2 for the remaining CO_2 emissions (during both day and night) must exist. Plausible sources are net ecosystem respiration and calcification, which should both increase during daytime warming. Florida Bay seagrasses are highly productive, with underwater eddy covariance studies (Long et al. 2015) showing large benthic O_2 production at Bob Allen (25 mmol O_2 m^{-2} d^{-1}, or 0.29 μmol O_2 m^2 s^{-1}). However, seagrass productivity is only one component of net ecosystem metabolism, which is in turn just one factor contributing to net CO_2 production or consumption and ultimate exchange with the atmosphere. As a case in point, seagrass beds elsewhere in Florida Bay have been found to be net heterotrophic (Van Dam et al. 2019*a*), offering a partial explanation for prior observations of pCO_2 above (Millero et al. 2001) or near (Yates et al. 2007) equilibrium with the atmosphere in this area. Likewise, Berg et al. (2019) attributed a shift from net O_2 production during the spring to O_2 consumption in the summer (in a temperate *Zostera marina* meadow) to temperature-sensitive increases in ecosystem respiration during the warm summer months.

We also suspect a variety of other benthic processes as CO_2 sources/sinks affecting CO_2 flux, including calcification/carbonate dissolution, denitrification, and net sulfur biogeochemistry. First, while Florida Bay overall should be a net producer of carbonate minerals (Bosence 1989), only some regions are indeed net calcifying (Yates and Halley 2006; Turk et al. 2015), with other regions apparently net dissolving (Van Dam et al. 2019*a*). Assuming all CO_2 produced or consumed by calcification exchanges with the atmosphere, recent estimates of carbonate dissolution (Van Dam et al. 2019*a*) and precipitation (Turk et al. 2015) in this region can be used to explain air–water CO_2 fluxes of −0.14 to 0.57 μmol CO_2 m^{-2} s^{-1}, respectively. These estimates are well within range of our CO_2 flux observations, indicating that carbonate precipitation may be responsible for the net CO_2 emission at this seagrass meadow. Next, organic carbon respiration via nitrate reduction (denitrification, dissimilatory nitrate reduction to ammonium) is an important heterotrophic pathway in seagrass sediments. While the CO_2 produced via denitrification is likely orders of magnitude below measured CO_2 flux (Eyre and Ferguson 2002; Welsh et al. 2000), the alkalinity generated by net denitrification may be important to the carbonate equilibria of overlying water. Likewise, while rates of sulfate reduction are high in Florida Bay (Walter et al. 2007), CO_2 produced by this mechanism appears to be at rates far below our CO_2 flux measurements. Nevertheless, the reoxidation of sulfide in the root zone enhances carbonate dissolution (Ku et al. 1999), with uncertain impacts on water-column carbonate chemistry.

Given the recent interest in the carbon sequestration potential of seagrasses (Duarte et al. 2005, 2010; Fourqurean et al. 2012*a*), and the growing recognition that $CaCO_3$ reactions must be included in "blue carbon" accounting (Mazarrasa et al. 2015; Macreadie et al. 2017; Howard et al. 2018), there is a clear need for studies combining direct measurements of CO_2 flux with determinations of carbonate precipitation/dissolution, as well as sulfate and nitrate reduction rates. The bulk of measured CO_2 emissions in this study cannot yet be attributed to a direct biogeochemical source, providing further motivation for such studies.

Physical drivers of the gas transfer velocity (k_w)

In the present study, we estimated k_w using heat as a proxy for gas transfer and found that it agreed reasonably well with k_w parameterized by wind speed (k_{W14}, k_{J08}) or a combination of wind, current speed, and water depth (k_{Ho16}). On average, the difference between k_W and k_{W14} was not significantly different from zero (i.e., $k_w - k_{W14} = -0.98 \pm 8.6$ cm h^{-1} [$\bar{x} \pm$ SD]). However, these parameterizations all tended to overpredict calculated k_w especially at higher friction velocity (u_*) and ΔT (Fig. 8b,c). Prior estimates of k_w using similar heat-transfer approaches have largely found this k_w to instead exceed the directly measured gas transfer velocity, indicating that the apparent gas transfer suppression in this study is not an artifact. Other studies in stratified lakes (MacIntyre et al. 2010), rivers (Berg and Pace 2017), Everglades freshwater wetlands (Ho et al. 2018*b*), and Amazon floodplains (Polsenaere et al. 2013) have observed similar gas transfer suppression during periods of heating under light to moderate winds. It is likely that this gas transfer suppression was caused by thermal stratification, generated during the day by large buoyancy fluxes into the water (Fig. 6c). This thermal stratification will dissipate when buoyancy fluxes reverses sign after dusk.

However, some time is required for stratification to be broken down by net heat fluxes as well as wind- and current-driven shear, eventually causing air and water temperature to approach equilibrium. Therefore, while we did observe a clear diel pattern in ΔT when plotted as a climatological hourly mean (Fig. 6d), there were many occasions where positive ΔT anomalies persisted through the evening and night hours (not shown). Accordingly, we observed that these periods of gas transfer suppression ($k_w < k_{W14}$) occurred both during the day and at night, when ΔT has not yet decreased. This effect is illustrated in Fig. 9c–f, where significant relationships exist between both u_*, w_{*w}, and k_w. While the nighttime correlation between w_{*w}, and k_w is significant, there is no relationship during the day, when large buoyancy fluxes into surface water (Fig. 6c) suppressed convective mixing. Furthermore, we observed decreases in k_w with increasing ΔT (at a given u_* or w_{*w}), such that k_w was rarely above 10 cm h^{-1} when ΔT exceeded ~ 4°C.

A closer examination of atmospheric stability conditions provides further evidence for the inferred suppression of gas transfer. As discussed above, atmospheric conditions were frequently in the UVCN zone, where $-0.1 < z/L < 0$. Such conditions may enhance gas transfer via periodic energetic downdrafts adding turbulence to the air–water interface (Smedman et al. 2007; Sahlée et al. 2008; Andersson et al. 2018). In line with previous findings, we indeed found the greatest departure of k_w from k_{W14} when z/L was in intermediate, UVCN conditions (Fig. 9b). This deviation from prediction occurred in the positive direction (k_w enhancement) when ΔT was low, and in the negative direction (k_w suppression) when ΔT exceeded 2–3°C. Wind speed was also relatively high during UVCN conditions (Fig. 9a), but could not explain the deviation of k_w from prediction, because k_w–k_{W14} was not clearly positive or negative in the UVCN zone under elevated U_{10}. While convection and wind-shear appeared to be dominant drivers of CO_2 and latent heat fluxes, the greatest convective enhancement occurred under UVCN conditions. Future studies should more directly address the combined effects of water-side convection and UVCN conditions on turbulent exchanges in shallow water.

Collectively, our findings suggest buoyancy-driven suppression of gas transfer during the day (and convective enhancement at night). This buoyant suppression was broken down in the late afternoon by relatively large latent heat fluxes out of the water (Fig. 6b), which acted to reverse thermal stratification via convective overturn (negative buoyancy flux). These day-time latent heat fluxes imply similarly large evaporative water losses, which should increase the salinity at the sea surface microlayer (Asher et al. 2014). Subsequent density-driven overturn should then act to restore a stable density structure. However, these large latent heat fluxes out of the water also coincided with the greatest under-prediction of k_w relative to k_{W14} (between 15:00 h and 20:00 h, not shown), suggesting continued gas transfer suppression despite latent heat flux-driven salinization of the sea surface microlayer. These unstable, evaporation-driven, density anomalies can be maintained near the sea surface due to intralayer tension (Wurl et al.

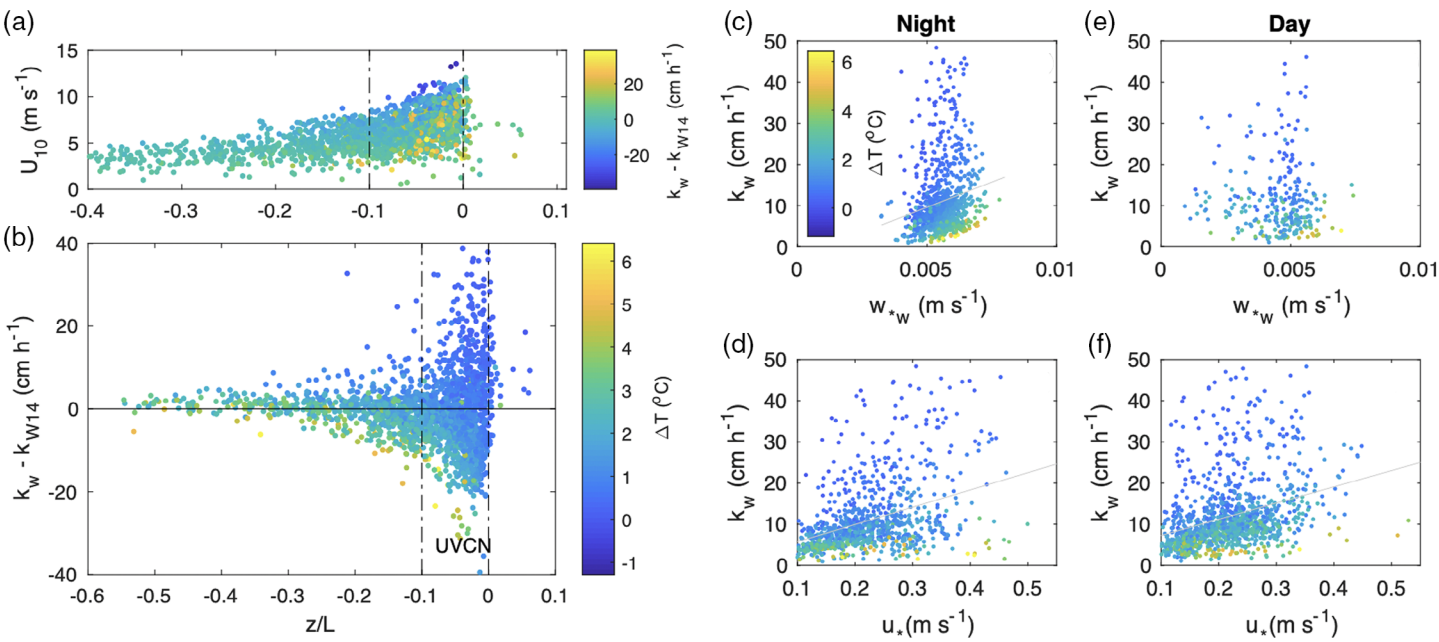

Fig. 9. Interaction between UVCN conditions and thermal stratification, including scatter plot of z/L vs. k_w–k_{W14} (**b**), and U_{10} (**a**). Points are colored by k_w–k_{W14} in (**a**), and by ΔT in (**b**). Dotted vertical lines represent UVCN conditions ($-0.1 < z/L < 0$). Scatter plots for day (right) and night (left) w_{*w} (**c**, **d**), u_* (**e**, **f**), and k_w, with the points colored by ΔT. Regression lines are not shown for (**e**) because the slope was not significantly different from zero ($p > 0.05$).

2019), perhaps allowing the larger buoyant structure to continue to dampen gas transfer. This is despite the expected effect of density-driven overturn, which should enhance vertical mixing and turbulent exchange.

Together, our results indicate that turbulent fluxes from these shallow waters cannot be explained by a simple stagnant boundary layer model, whereby air–water gas exchange is rate-limited by diffusion across a thin boundary layer. Instead, a more apt conceptual model may be one of eddy diffusion (Lamont and Scott 1970; Wang et al. 2015), whereby gas transfer is driven by the cascade of energy transfer toward molecular dissipation (Wanninkhof et al. 2009; Garbe et al. 2014). The findings of this study, based on direct eddy covariance measurements of CO_2 flux, contribute to our understanding of the physical process of gas transfer, specifically the balance between shear and convective forcing in shallow, coastal waters. Future studies can build on this work by making water-side pCO_2 measurements, facilitating the direct calculations of gas transfer velocity.

Evaporation-precipitation balance in Florida Bay

The clear trend of increasing salinity over the study period, with the transition *into* the wet season (Fig. 3b), may seem counterintuitive but fits well with the current understanding of Florida Bay's water balance. Net surface water inputs to Florida Bay are small, and have little effect on salinity trends, especially in central and western regions of the bay (Nuttle et al. 2000). Here, the water budget can be considered as a simple evaporation-precipitation balance (Nuttle et al. 2000; Swart and Price 2002; Price et al. 2007), where any small changes in water level are compensated for by slow tidal exchange across sub-basins. Over our study period, cumulative evaporation and precipitation were 518.6 mm and 172 mm, respectively, creating a water deficit of 346.6 mm. Water lost to evaporation is replaced through lateral exchange with adjacent basins and eventually the Gulf of Mexico (Lee et al. 2006, 2008). Morphologically, Florida Bay is a collection of broad and shallow basins surrounded by mud banks (Fig. 1). These banks are cut by narrow channels, which serve as the only path for cross-basin water exchange (Wang et al. 1994), causing long water residence times, of $\sim$6–12 months (Lee et al. 2006). Any change in the size of these channels will affect water residence times, causing variable impacts of the evaporation-precipitation balance on salinity trends.

An additional factor affecting the local water balance is clearly the rate of evaporation (LE), which if not balanced by lateral mixing would have caused salinity to rise by 13.5, rather than the observed change of 4.9. While net solar radiation can be a good predictor of evaporation over longer, monthly and seasonal time scales in Florida Bay (Price et al. 2007) and in large and shallow lakes like Taihu (Lee et al. 2014) and Lake Erie (Shao et al. 2015), we found no such relationship between latent heat flux and net solar radiation. Instead, we found that peak latent heat flux (at $\sim$16:00 h) occurred nearly 4 h after the mid-day peak in net solar radiation (Fig. 6). Such time lags between latent heat flux and net solar radiation have been documented previously in eastern Florida Bay (Price et al. 2007) and in shallow lakes (Czikowsky et al. 2018). Instead, we found that latent heat fluxes were driven by convective (ΔT, w_{*w}) and shear (U_{10}) forcing in conjunction with vapor pressure deficit. This has been observed previously in a subtropical reservoir (Liu et al. 2009), and related to frontal patterns which can deliver either cold or dry air (enhancing latent heat flux) or warm and moist air (suppressing latent heat flux). We also found that diel trends in latent heat fluxes were opposite of those observed at temperate (Shao et al. 2015; Rey-sánchez et al. 2017) and subtropical (Liu et al. 2009) sites where latent heat flux is typically greater at night. Instead, the high daytime ΔT caused latent heat fluxes to be similar to other tropical sites (Polsenaere et al. 2013). Last, we show that large buoyancy fluxes into the water during the day (11:00 h peak of 4.6×10^{-7} m^2 s^{-3}) effectively suppress daytime latent heat fluxes. At night, buoyancy loss from the water (nighttime average of -1.3×10^{-7} m^2 s^{-3}) drives convective enhancement of latent heat flux (and CO_2 flux).

In summary, observed latent heat flux trends were in stark contrast with other temperate (Shao et al. 2015; Rey-sánchez et al. 2017) and subtropical (Liu et al. 2009) sites where latent heat flux is greatest at night, driven by a cooling of the air relative to the water. While we were able to quantitatively explore the drivers of latent heat flux, and link it with seasonal variations in salinity, more data are required to understand the complete, annual, evaporation-precipitation balance. Additional studies using modeling approaches or rainfall isotopic measurements could explore the ultimate fate of evaporative water losses from Florida Bay, and whether it is of any significance to the freshwater budget of the Florida Everglades.

Regional significance

As discussed in "Temporal trends in air–water CO_2/latent heat fluxes and associated parameters" section, the unique diel excursion in ΔT at this site (greater ΔT during the day than at night) appears to be related to the marine origin of air reaching central Florida Bay. Due to the presence of the easterly "trade" winds at this latitude, air parcels arriving at this site are near thermal equilibrium with the coastal ocean. This, in conjunction with the shallow water depth (< 2 m) and intense solar heating, causes diel trends in ΔT to be dictated by water temperature rather than air temperature. We document the importance of this diel excursion in ΔT on: (1) increasing pCO_2 (lowering CO_2 solubility), (2) buoyancy-driven daytime suppression of turbulent air-water exchange, and (3) nighttime convective enhancement of turbulent fluxes. These factors are likely important at other shallow, subtropical sites, with relatively stable air temperature. In contrast, at shallow coastal sites adjacent to large land masses,

continental weather patterns may cause air temperature to be variable, relative to water temperature, causing an opposite diel trend in ΔT (increasing during the night and decreasing during the day). This may be one mechanism by which turbulent fluxes at coastal sites fringing land may be fundamentally different from those at ocean-dominated sites. We expect that air mass origin (either maritime or continental) will have a significant effect on air–water transfer of gas and energy in shallow coastal waters. This topic could be addressed with simple analyses of existing eddy covariance data sets.

Conclusion

We report on the first direct measurements of air–water exchange of CO_2 and heat over a tropical seagrass ecosystem. Against convention, CO_2 flux was largely positive (out of the water), with peak emissions during warm afternoon hours. A more complete explanation of these CO_2 emissions will require water column measurements along with a full annual cycle of direct CO_2 flux determinations by eddy covariance and water pCO_2 measurements. Nevertheless, it appears that $\sim 23\%$ of the daytime increases in CO_2 flux (likewise, the night-time decrease in CO_2 flux) can be ascribed to the direct, thermodynamic effect of rising water temperature on decreasing CO_2 solubility. The remaining CO_2 emissions may be the combined product of net ecosystem heterotrophy, carbonate precipitation/dissolution, sediment denitrification, and net sulfur biogeochemistry. The relative importance of each process on the carbonate equilibria and ultimate air–water CO_2 exchange is presently unknown. However, it is clear that temperature played a key role in enhancing latent heat fluxes, which generated a water deficit over the short study period of 346.6 mm, causing dramatic increases in salinity. Our correlation analysis indicates that evaporation rates cannot be predicted by a simple relationship with net radiation (as previously assumed), but instead respond to a complex interaction between vapor pressure deficit, air–water temperature differences (ΔT), and convective (w_{*w}) as well as wind (U_{10}) forcing. As elevated salinity and temperature have been associated with historic seagrass die-offs in Florida Bay and elsewhere, our findings should help ecosystem managers predict when and where future die-off events may occur. In other words, Florida Bay's water budget cannot be understood through solar radiation alone. We describe a suite of factors that should instead be used to forecast changes in temperature and salinity over daily to weekly time scales. Last, we showed that it is possible to estimate the gas transfer velocity (k_w) using heat exchange as a proxy for gas exchange. Using this new approach, we found that k_w was less than predicted by commonly used empirical parameterizations based on wind alone or wind and water velocity. This dampening of k_w became more prominent with increased daytime ΔT, suggesting that this gas transfer suppression is related to thermal stratification at the sea surface. We point to the apparent contradiction of thermal gas transfer suppression during periods of rapid evaporation, when salinization at the sea surface should instead enhance gas transfer via density-driven vertical mixing. Our results suggest the competing roles of buoyancy fluxes and latent heat fluxes as modulators of gas transfer in shallow, tropical waters. Future studies could build on this work, with water-side measurements of pCO_2, temperature, and salinity to further address this question.

Together, these findings show that air–water CO_2 exchange in shallow, tropical seagrass ecosystems does not function as other submerged vegetated environments in deeper or more temperate waters. Our results point to temperature as a critical factor governing: (1) evaporative water loss, (2) diel cycles in CO_2 flux (as well as pCO_2), and (3) the physical process of air–water gas transfer. By investigating the factors affecting air–sea CO_2 and H_2O exchange in tropical seagrass meadows, this study will improve our understanding of these important ecosystems in broader regional and global cycles of carbon and water.

Data availability statement

All data sets generated during this project are published on the data sharing repository Figshare (https://doi.org/10.6084/m9.figshare.7707029.v1). Further requests for data or methods sharing can be directed toward the corresponding author.

References

Andersson, A., A. Sjöblom, E. Sahlée, E. Falck, and A. Rutgersson. 2018. Enhanced air–sea exchange of heat and carbon dioxide over a high Arctic Fjord during unstable very-close-to-neutral conditions. Boundary Layer Meteorol. **170**: 471–488. doi:10.1007/s10546-018-0408-9

Armitage, A. R., and J. W. Fourqurean. 2016. Carbon storage in seagrass soils: Long-term nutrient history exceeds the effects of near-term nutrient enrichment. Biogeosciences **13**: 313–321. doi:10.5194/bg-13-313-2016

Asmala, E., C. Gustafsson, D. Krause-Jensen, A. Norkko, H. Reader, P. A. Staehr, and J. Carstensen. 2019. Role of eelgrass in the coastal filter of contrasting Baltic Sea environments. Estuaries Coast. **42**: 1882–1895. doi:10.1007/s12237-019-00615-0

Asher, W., A. Jessup, and C. Dan. 2014. Stable near-surface ocean salinity stratifications due to evaporation observed during STRASSE. Journal of Geophysical Research: Oceans, Oceans, 6121–6139. https://doi.org/10.1002/2014JC010105

Attard, K. M., I. F. Rodil, R. N. Glud, P. Berg, J. Norkko, and A. Norkko. 2019. Seasonal ecosystem metabolism across shallow benthic habitats measured by aquatic eddy covariance. Limnol. Oceanogr.: Lett. **4**: 79–86. doi:10.1002/lol2.10107

Berg, P., and M. L. Pace. 2017. Continuous measurement of air-water gas exchange by underwater eddy covariance. Biogeosciences **14**: 1–27. doi:10.5194/bg-14-5595-2017

Berg, P., M. L. Delgard, P. Polsenaere, K. J. Mcglathery, S. C. Doney, and A. C. Berger. 2019. Dynamics of benthic metabolism, O_2, and pCO_2 in a temperate seagrass meadow. Limnol. Oceanogr. **64**: 1–19. doi:10.1002/lno.11236

Borum J., O. Pedersen, T. M. Greve, T. A. Frankovich, J. C. Zieman, J. W. Fourqurean, and C. J. Madden 2005. The potential role of plant oxygen and sulphide dynamics in die-off events of the tropical seagrass, Thalassia testudinum. Journal of Ecology **93**: (1) 148–158. http://dx.doi.org/10.1111/j.1365-2745.2004.00943.x

Bosence, D. W. J. 1989. Biogenic carbonate production in Florida Bay. Bull. Mar. Sci. **44**: 419–433.

Czikowsky, M. J., S. MacIntyre, E. W. Tedford, J. Vidal, and S. D. Miller. 2018. Effects of wind and buoyancy on carbon dioxide distribution and air-water flux of a stratified temperate lake. J. Geophys. Res. Biogeosci. **123**: 2305–2322. doi:10.1029/2017JG004209

Duarte, C. M., J. J. Middelburg, and N. Caraco. 2005. Major role of marine vegetation on the oceanic carbon cycle. Biogeosciences **2**: 1–8. doi:10.5194/bg-2-1-2005

Duarte, C. M., N. Marbà, E. Gacia, J. W. Fourqurean, J. Beggins, C. Barrón, and E. T. Apostolaki. 2010. Seagrass community metabolism: Assessing the carbon sink capacity of seagrass meadows. Global Biogeochem. Cycles **24**: 1–8. doi:10.1029/2010GB003793

DuFore, C. 2011. Spatial and temporal variations in the air-sea carbon dioxide fluxes of Florida Bay. Thesis. Master of Science, College of Marine Science, University of South Florida.

Eyre, B. D., and A. J. P. Ferguson. 2002. Comparison of carbon production and decomposition, benthic nutrient fluxes and denitrification in seagrass, phytoplankton, benthic microalgae- and macroalgae-dominated warm-temperate Australian lagoons. Marine Ecology Progress Series, Marine Ecology Progress Series, **229**: 43–59. https://doi.org/10.3354/meps229043

Foken T., M. Aubinet, and R. Leuning. (2012). The Eddy Covariance Method. In: Aubinet M., Vesala T., Papale D. (eds) Eddy Covariance. Springer Atmospheric Sciences. Springer, Dordrecht. https://doi.org/10.1007/978-94-007-2351-1_1.

Fourqurean, J., J. Zieman, and G. Powell. 1992. Phosphorus limitation of primary production in Florida Bay: Evidence from C:N:P ratios of the dominant seagrass *Thalassia testudinum*. Limnol. Oceanogr. **37**: 162–171.https://doi.org/10.1007/978-94-007-2351-1_1

Fourqurean, J. W., and others. 2012*a*. Seagrass ecosystems as a globally significant carbon stock. Nat. Geosci. **5**: 505–509. doi:10.1038/ngeo1477

Fourqurean, J. W., G. A. Kendrick, L. S. Collins, R. M. Chambers, and M. A. Vanderklift. 2012*b*. Carbon, nitrogen and phosphorus storage in subtropical seagrass meadows: Examples from Florida Bay and Shark Bay. Mar. Freshw. Res. **63**: 967–983. doi:10.1071/MF12101

Garbe C. S. et al. (2014). Transfer Across the Air-Sea Interface. In: Liss P.S., Johnson M.T. (eds) Ocean-Atmosphere Interactions of Gases and Particles. Springer Earth System Sciences. Springer, Berlin, Heidelberg. https://doi.org/10.1007/978-3-642-25643-1_2.

Green, E. P., and F. T. Short. 2003. World atlas of seagrasses, v. **310**. California Univ. Press.

Ho David T., Coffineau Nathalie, Hickman Benjamin, Chow Nicholas, Koffman Tobias, and Schlosser Peter 2016. Influence of current velocity and wind speed on air-water gas exchange in a mangrove estuary. Geophysical Research Letters **43**: (8) 3813–3821. http://dx.doi.org/10.1002/2016gl068727

Ho, D. T., E. H. De Carlo, and P. Schlosser. 2018*a*. Air-sea gas exchange and CO_2 fluxes in a tropical coral reef lagoon. J. Geophys. Res. Oceans **123**: 8701–8713. doi:10.1029/2018JC014423

Ho, D. T., V. C. Engel, S. Ferrón, B. Hickman, J. Choi, and J. W. Harvey. 2018*b*. On factors influencing air-water gas exchange in emergent wetlands. J. Geophys. Res. Biogeosci. **123**: 178–192. doi:10.1002/2017JG004299

Holmquist, J. G., G. V. N. Powell, and S. M. Sogard. 1989. Sediment, water level and water temperature characteristics of Florida Bay's grass-covered mud banks. Bull. Mar. Sci. **44**: 348–364.

Howard, J. L., J. C. Creed, M. V. P. Aguiar, and J. W. Fouqurean. 2018. CO_2 released by carbonate sediment production in some coastal areas may offset the benefits of seagrass "Blue Carbon" storage. Limnol. Oceanogr. **63**: 160–172. doi:10.1002/lno.10621

Jeffery, C. D., D. K. Woolf, I. S. Robinson, and C. J. Donlon. 2007. One-dimensional modelling of convective CO_2 exchange in the Tropical Atlantic. Ocean Model. **19**: 161–182. doi:10.1016/j.ocemod.2007.07.003

Jiang Li-Qing, Cai Wei-Jun, and Wang Yongchen 2008. A comparative study of carbon dioxide degassing in river- and marine-dominated estuaries. Limnology and Oceanography **53**: (6) 2603–2615. http://dx.doi.org/10.4319/lo.2008.53.6.2603

Joesoef, A., W. J. Huang, Y. Gao, and W.-J. Cai. 2015. Air-water fluxes and sources of carbon dioxide in the Delaware Estuary: Spatial and seasonal variability. Biogeosciences **12**: 6085–6101. doi:10.5194/bg-12-6085-2015

Jonsson, A., J. Åberg, A. Lindroth, and M. Jansson. 2008. Gas transfer rate and CO_2 flux between an unproductive lake and the atmosphere in northern Sweden. J. Geophys. Res. Biogeosci. **113**: 1–13. doi:10.1029/2008JG000688

Kennedy, H., J. Beggins, C. M. Duarte, J. W. Fourqurean, M. Holmer, N. Marbá, and J. J. Middelburg. 2010. Seagrass sediments as a global carbon sink: Isotopic constraints. Global Biogeochem. Cycles **24**: 1–8. doi:10.1029/2010GB003848

Kljun, N., P. Calanca, M. W. Rotach, and H. P. Schmid. 2015. A simple two-dimensional parameterisation for Flux Footprint Prediction (FFP). Geosci. Model Dev. **8**: 3695–3713. doi:10.5194/gmd-8-3695-2015

Koch, M. S., S. Schopmeyer, C. Kyhn-Hansen, and C. J. Madden. 2007. Synergistic effects of high temperature and sulfide on tropical seagrass. J. Exp. Mar. Biol. Ecol. **341**: 91–101. doi:10.1016/j.jembe.2006.10.004

Ku, T. C. W., L. M. Walter, M. L. Coleman, R. E. Blake, and A. M. Martini. 1999. Coupling between sulfur recycling and syndepositional carbonate dissolution: Evidence from oxygen and sulfur isotope composition of pore water sulfate, South Florida Platform, U.S.A. Geochim. Cosmochim. Acta **63**: 2529–2546. doi:10.1016/S0016-7037(99)00115-5

Lamont, J. C., and D. S. Scott. 1970. Eddy cell model of mass transfer into the surface of a turbulent liquid. AIChE J. **16**: 513–519. doi:10.1002/aic.690160403

Large W. G., and S. Pond 1981. Open Ocean Momentum Flux Measurements in Moderate to Strong Winds. Journal of Physical Oceanography **11**: (3) 324–336. http://dx.doi.org/10.1175/1520-0485(1981)011<0324:oomfmi>2.0.co;2

Lee, T. N., E. Johns, N. Melo, R. H. Smith, P. Ortner, and D. Smith. 2006. On Florida Bay hypersalinity and water exchange. Bull. Mar. Sci. **79**: 301–327.

Lee, T. N., N. Melo, E. Johns, C. Kelble, R. H. Smith, and P. Ortner. 2008. On water renewal and salinity variability in the northeast subregion of Florida Bay. Bull. Mar. Sci. **82**: 83–105.

Lee, X., and others. 2014. The taihu eddy flux network: An observational program on energy, water, and greenhouse gas fluxes of a large freshwater lake. Bull. Am. Meteorol. Soc. **95**: 1583–1594. doi:10.1175/BAMS-D-13-00136.1

Liu, H., Y. Zhang, S. Liu, H. Jiang, L. Sheng, and Q. L. Williams. 2009. Eddy covariance measurements of surface energy budget and evaporation in a cool season over southern open water in Mississippi. J. Geophys. Res. **114**: 1–13. doi:10.1029/2008JD010891

Long, M., P. Berg, and J. Falter. 2015. Seagrass metabolism across a productivity gradient using the eddy covariance, Eulerian control volume, and biomass addition techniques. J. Geophys. Res. Oceans **120**: 2676–2700. doi:10.1002/2014JC010441

MacIntyre, S., A. Jonsson, M. Jansson, J. Aberg, D. E. Turney, and S. D. Miller. 2010. Buoyancy flux, turbulence, and the gas transfer coefficient in a stratified lake. Geophys. Res. Lett. **37**: 2–6. doi:10.1029/2010GL044164

Macreadie, P. I., O. Serrano, D. T. Maher, C. M. Duarte, and J. Beardall. 2017. Addressing calcium carbonate cycling in blue carbon accounting. Limnol. Oceanogr.: Lett. **2**: 195–201. doi:10.1002/lol2.10052

Macreadie, P. I., and others. 2019. The future of blue carbon science. Nat. Commun. **10**: 1–13. doi:10.1038/s41467-019-11693-w

Mauder Matthias, and Foken Thomas 2006. Impact of post-field data processing on eddy covariance flux estimates and energy balance closure. Meteorologische Zeitschrift **15**: (6) 597–609. http://dx.doi.org/10.1127/0941-2948/2006/0167

Mazarrasa, I., and others. 2015. Seagrass meadows as a globally significant carbonate reservoir. Biogeosciences **12**: 4993–5003. doi:10.5194/bg-12-4993-2015

Mørk, E. T., M. Sejr, P. A. Stæhr, and L. L. Sørensen. 2016. Temporal variability of air-sea CO2 exchange in a low-emission estuary. Estuarine, Coastal and Shelf Science. **176**: 1–11. https://doi.org/10.1016/j.ecss.2016.03.022

McKenna, S. P., and W. R. McGillis. 2004. The role of free-surface turbulence and surfactants in air-water gas transfer. Int. J. Heat Mass Transf. **47**: 539–553. doi:10.1016/j.ijheatmasstransfer.2003.06.001

Millero, F., W. Hiscock, R. Huang, M. Roche, J. Zhang, Frank J. Millero, William T Hiscock , Fen Huang, and J. Z. Z. Mary Roche, et al. 2001. Seasonal Variation of the Carbonate System in Florida Bay. Bulletin of Marine Science, **68**(1): 101–123.

Mørk, E. T., L. L. Sørensen, B. Jensen, and M. K. Sejr. 2014. Air–sea CO_2 gas transfer velocity in a shallow estuary. Boundary Layer Meteorol. **151**: 119–138. doi:10.1007/s10546-013-9869-z

Nellemann, C., E. Corcoran, C. M. Duarte, L. Valdés, C. De Young, L. Fonseca, and G. Grimsditch. 2009. Blue carbon. A rapid response assessment. United Nations Environment Programme, GRID-Arenal, p. 78.

Nuttle, W. K., J. W. Fourqurean, B. J. Cosby, J. C. Zieman, B. Robblee, and F. Bay. 2000. Influence of net freshwater supply on salinity in Florida Bay. Water Resources Research, **36** (7): 1805–1822.

Perez, D. I., S. R. Phinn, C. M. Roelfsema, E. Shaw, L. Johnston, and J. Iguel. 2018. Primary production and calcification rates of algae-dominated reef flat and seagrass communities. J. Geophys. Res. Biogeosci. **123**: 2362–2375. doi:10.1029/2017JG004241

Podgrajsek, E., E. Sahlée, and A. Rutgersson. 2015. Diel cycle of lake-air CO_2 flux from a shallow lake and the impact of waterside convection on the transfer velocity. J. Geophys. Res. Biogeosci. **120**: 29–38. doi:10.1002/2014JG002781

Polsenaere, P., and others. 2012. Spatial and temporal CO_2 exchanges measured by eddy covariance over a temperate intertidal flat and their relationships to net ecosystem production. Biogeosciences **9**: 249–268. doi:10.5194/bg-9-249-2012

Polsenaere, P., J. Deborde, G. Detandt, L. O. Vidal, M. A. P. Pérez, V. Marieu, and G. Abril. 2013. Thermal enhancement of gas transfer velocity of CO_2 in an Amazon floodplain lake revealed by eddy covariance measurements. Geophys. Res. Lett. **40**: 1734–1740. doi:10.1002/grl.50291

Price, R. M., W. K. Nuttle, B. J. Cosby, and P. K. Swart. 2007. Variation and uncertainty in evaporation from a subtropical estuary: Florida Bay. Estuaries Coast. **30**: 497–506. doi:10.1007/BF02819396

Rey-sánchez, A. C., G. Bohrer, T. H. Morin, D. Shlomo, and G. Mirfenderesgi. 2017. Evaporation and CO_2 fluxes in a coastal reef: An eddy covariance approach. Ecosyst. Health Sustain. **3**: 1392830. doi:10.1080/20964129.2017.1392830

Ribas-Ribas, M., F. Helleis, J. Rahlff, and O. Wurl. 2018. Air-sea CO_2-exchange in a large annular wind-wave tank and the effects of surfactants. Front. Mar. Sci. **5**: 1–16. doi:10.3389/fmars.2018.00457

Robblee, M., and others. 1991. Mass mortality of the tropical seagrass *Thalassia testudinum* in Florida Bay (USA). Mar. Ecol. Prog. Ser. **71**: 297–299. doi:10.3354/meps071297

Röhr, M. E., and others. 2018. Blue carbon storage capacity of temperate eelgrass (*Zostera marina*) meadows. Global Biochem. Cycles **32**: 1457–1475. doi:10.1029/2018GB005941

Rutgersson, A., A. Smedman, and E. Sahle. 2011. Oceanic convective mixing and the impact on air-sea gas transfer velocity. Geophys. Res. Lett. **38**: 1–5. doi:10.1029/2010GL045581

Sahlée, E., A.-S. Smedman, U. Högström, and A. Rutgersson. 2008. Reevaluation of the bulk exchange coefficient for humidity at sea during unstable and neutral conditions. J. Phys. Oceanogr. **38**: 257–272. doi:10.1175/2007jpo3754.1

Shao, C., and others. 2015. Diurnal to annual changes in latent, sensible heat, and CO_2 fluxes over a Laurentian Great Lake: A case study in Western Lake Erie. J. Geophys. Res. Biogeosci. **120**: 1587–1604. doi:10.1002/2015JG003025

Smedman, A.-S., U. Hogstrom, J. Hunt, and E. Sahlée. 2007. Heat/mass transfer in the slightly unstable atmospheric surface layer. Q. J. R. Meterol. Soc. **133**: 37–51. doi:10.1002/qj.7

Swart, P. K., and R. Price. 2002. Origin of salinity variations in Florida Bay. Limnol. Oceanogr. **47**: 1234–1241. doi:10.4319/lo.2002.47.4.1234

Smith, M. J., D. T. Ho, C. S. Law, J. McGregor, S. Popinet, and P. Schlosser. 2011. Uncertainties in gas exchange parameterization during the SAGE dual-tracer experiment. Deep Sea Research Part II: Topical Studies in Oceanography. **58**(6): 869–881. https://doi.org/10.1016/j.dsr2.2010.10.025

Takahashi, T., J. Olafsson, J. G. Goddard, D. W. Chipman, and S. C. Sutherland. 1993. Seasonal variation of CO_2 and nutrients in the high latitude surface oceans: A comparative study. Global Biochem. Cycles **7**: 843–878.

Tokoro, T., A. Watanabe, H. Kayanne, and K. Nadaoka. 2007. Measurement of air–water CO_2 transfer at four coastal sites using a chamber method. J. Mar. Syst. **66**: 140–149. doi:10.1016/j.jmarsys.2006.04.010

Tokoro, T., S. Hosokawa, E. Miyoshi, K. Tada, K. Watanabe, S. Montani, H. Kayanne, and T. Kuwae. 2014. Net uptake of atmospheric CO_2 by coastal submerged aquatic vegetation. Glob. Chang. Biol. **20**: 1873–1884. doi:10.1111/gcb.12543

Tokoro, T., K. Watanabe, K. Tada, and T. Kuwae. (2019). Air-Water CO_2 Flux in Shallow Coastal Waters: Theory, Methods, and Empirical Studies. In Blue Carbon in Shallow Coastal Ecosystems (pp. 153–184). Springer, Singapore.

Turk, D., and others. 2015. Community metabolism in shallow coral reef and seagrass ecosystems, lower Florida keys. Mar. Ecol. Prog. Ser. **538**: 35–52. doi:10.3354/meps11385

Upstill-Goddard, R. C. 2006. Air–sea gas exchange in the coastal zone. Estuar. Coast. Shelf Sci. **70**: 388–404. doi:10.1016/j.ecss.2006.05.043

Van Dam, B. R., C. Lopes, C. L. Osburn, and J. W. Fourqurean. 2019*a*. Net heterotrophy and carbonate dissolution in two subtropical seagrass meadows. Biogeosciences **16**: 4411–4428. doi:10.5194/bg-2019-191

Van Dam, B. R., J. B. Edson, and C. Tobias. 2019*b*. Parameterizing air-water gas exchange in the shallow, microtidal New River Estuary. J. Geophys. Res. Biogeosci. **124**: 2351–2363. doi:10.1029/2018JG004908

Walter, L. M., T. C. W. Ku, K. Muehlenbachs, W. P. Patterson, and L. Bonnell. 2007. Controls on the $\delta^{13}C$ of dissolved inorganic carbon in marine pore waters: An integrated case study of isotope exchange during syndepositional recrystallization of biogenic carbonate sediments (South Florida Platform, USA). Deep-Sea Res. Part II Top. Stud. Oceanogr. **54**: 1163–1200. doi:10.1016/j.dsr2.2007.04.014

Wang, B., Q. Liao, J. H. Fillingham, and H. A. Bootsma. 2015. On the coefficients of small eddy and surface divergence models for the air-water gas transfer velocity. J. Geophys. Res. Oceans **120**: 2129–2146. doi:10.1002/2014JC010253

Wang, J. D., J. Van De Kreeke, N. Krishnan, and D. Smith. 1994. Wind and tide response in Florida Bay. Bull. Mar. Sci. **54**: 579–601.

Wanninkhof, R. 2014. Relationship between wind speed and gas exchange over the ocean revisited. Limnol. Oceanogr.: Methods **12**: 351–362. doi:10.4319/lom.2014.12.351

Wanninkhof, R., W. E. Asher, D. T. Ho, C. Sweeney, and W. R. McGillis. 2009. Advances in quantifying air-sea gas exchange and environmental forcing. Ann. Rev. Mar. Sci. **1**: 213–244. doi:10.1146/annurev.marine.010908.163742

Webb, E. K., G. I. Pearman, and R. Leuning. 1980. Correction of flux measurements for density effects due to heat and water vapour transfer. Q. J. R. Meteorol. Soc. **106**: 85–100.

Wurl, O., W. M. Landing, N. I. H. Mustaffa, M. Ribas-Ribas, C. R. Witte, and C. J. Zappa. 2019. The Ocean's Skin Layer in the Tropics. Journal of Geophysical Research: Oceans, **124** (1): 59–74. https://doi.org/10.1029/2018JC014021

Yates, K. K., C. Dufore, N. Smiley, C. Jackson, and R. B. Halley. 2007. Diurnal variation of oxygen and carbonate system

parameters in Tampa Bay and Florida Bay. Mar. Chem. **104**: 110–124. doi:10.1016/j.marchem.2006.12.008

Yates, K. K., and R. B. Halley. 2006. Diurnal variation in rates of calcification and carbonate sediment dissolution in Florida Bay. Estuaries Coast. **29**: 24–39. doi:10.1007/BF02784696

Zappa, C. J., P. A. Raymond, E. A. Terray, and W. R. McGillis. 2003. Variation in surface turbulence and the gas transfer velocity over a tidal cycle in a macro-tidal estuary. Estuaries **26**: 1401–1415. doi:10.1007/BF02803649

Zieman, J. C., J. W. Fourqurean, and R. L. Iverson. 1989. Distribution, abundance and productivity of seagrasses and macroalgae in Florida Bay. Bull. Mar. Sci. **44**: 292–311.

Acknowledgments

This work was supported by the US National Science Foundation through the Florida Coastal Everglades Long-Term Ecological Research program under Grants DEB-1237517 and DEB-1832229 and additionally through DAAD (57429828) from funds of the German Federal Ministry of Education and Research (BMBF). We thank Sara Wilson and Mary Zeller for assistance in the lab and field. Mary Zeller also generously gave her time in reviewing this manuscript. We also appreciate the assistance of the National Parks Service, who allowed this equipment to be deployed in the Everglades National Park, under Permit number (EVER-2018-SCI-0072). Last, we appreciate the helpful comments during review, which significantly improved the final manuscript. This is contribution #180 from the Coastlines and Oceans Division of the Institute of Environment at Florida International University.

Conflict of Interest

None declared.

Submitted 28 October 2019
Revised 24 March 2020
Accepted 14 September 2020

Associate editor: Lauren Juranek